Research Article

Efficacy of Gold Photothermal-Activated Shape Memory Polyurethane

Christopher J. Ward,[1] Robert Tonndorf [1] Alicia Eustes,[1] Maria L. Auad [1,2] and Edward W. Davis [1,3,4]

[1]*Center for Polymers and Advanced Composites, Auburn University, USA*
[2]*Department of Chemical Engineering, Auburn University, USA*
[3]*Materials Research and Education Center, Auburn University, USA*
[4]*Department of Mechanical Engineering, Auburn University, USA*

Correspondence should be addressed to Edward W. Davis; ewd0001@auburn.edu

The addition of gold nanorods to a commercial polyurethane enabled shape memory behavior activation via infrared irradiation. The fraction of the set strain recovered was found to be dependent on the nanorod loading and irradiation intensity. A nanocomposite consisting of gold nanorods with an aspect ratio of ~3.25 and a diameter of ~11.5 nm and the polyurethane IROGRAN PS455-203 was prepared via a simple solution blending technique. Gold loadings up to 3.2 ppm by weight were evaluated. The glass transition temperature and melting point of the hard-segment phase was slightly depressed at the highest loading evaluated. Other thermal properties were not affected by the addition of gold nanorods. Also, the thermally activated shape memory behavior of the composite material was not affected by the presence of the gold nanorods.

1. Introduction

Smart materials that respond to a specific stimulus by recovering a previously set shape include both shape memory polymers [1, 2] (SMPs) and shape memory alloys (SMAs). Recovery is activated via stimuli, most often at a temperature transition of the material, and usually involves physical contact between the material and the agent that induces the alteration [2–10]. Shape memory alloys are widely used when high response temperatures or high stiffness is required, but the range of applications is limited. SMAs typically have recoverable strains less than 10%, are usually expensive, and have fixed transition temperatures. These limitations have motivated the development of SMPs. Some of the advantages of SMPs over SMAs include recoverable strains of hundreds of percent, much lower density, and much lower production costs.

Most importantly, the shape recovery of SMPs can be tailored to occur anywhere in a wide temperature range by adjusting the chemical structure of the network. Consequently, SMPs can be produced to function in biologically relevant temperature ranges. The significant strain recovery behavior and response temperature ranges of SMPs have been exploited to create novel medical devices and biological micro-electro-mechanical systems (bio-MEMS) [11–15]. For example, several widely used biomedical devices, such as catheters, ventricular assist bladders, and vascular grafts are fabricated using SMPs. Bio-MEMS devices have also led to minimally invasive surgery technology that features accurate blind release and placement capacity coupled with biocompatibility [16]. An equally important but less studied application for SMPs is in the area of drug delivery [17], specifically cancer therapy. Unfortunately, except for skin cancer, the vast majority of tumors are seated deep within the body. Activation of drug release with traditional SMPs would involve heating of body tissues in regions between the skin surface and the target tumor. Nonlocal heating not only raises the possibility of drug release in the surrounding

tissues, leading to unwanted side-effects, but can also lead to high-temperature induced necrosis of healthy tissues. The ability to remotely trigger drug release would potentially provide a means for tumor-targeted therapy.

In general, heating has been the external stimulus of choice for activating SMPs because of the intrinsic phase transitions occurring in polymers. The glassy, or melting, transition governs the temperature at which the material reverts to a predetermined, permanent shape after deformation and fixation of a temporary shape by cooling. Heating is a suitable trigger for activation of strain recovery in a wide range of SMPs. However, applying the thermal energy necessary to activate the shape transition in a contactless way remains a challenge. Several indirect heating methods have been studied to activate the shape memory effect of previously implanted devices without subsequent surgery, including inductive heating using oscillating magnetic fields [18, 19], radiofrequency irradiation [20], and electric fields [21]. Lendlein et al. worked on the development of nematic liquid crystal elastomers that can undergo light-induced shape changes due to conformational changes resulting from the absorption of light at a wavelength $\lambda > 260 \, nm$ [22]. However, the mechanism of response, while triggered by irradiation, is fundamentally chemical phenomena.

Excitation of the surface plasmon resonance (SPR) of metal nanoparticles provides another method for the remote heating of the polymer system. Surface plasmons are surface electromagnetic waves that propagate in a direction parallel to the metal/dielectric (or metal/vacuum) interface. By exciting a nanoparticle with the appropriate wavelength of electromagnetic energy, the electrons confined to this surface are repeatedly excited to higher energies from which they return to the ground state releasing energy as heat. This energy release results in highly localized heat generation. Significant research has been conducted to understand how to optimize this effect by changing the particle size and shape [23–27]. Using the stimulation of SPR of nanorods dispersed in SMPs offers three distinct advantages over other indirect heating methods. First, the SPR can be shifted to the NIR range by appropriate selection of the length to diameter (L/D) ratio of the particles; longer rods result in longer wavelength peak absorption [28, 29]. Shifting the wavelength to the NIR range, where body tissue is most transparent, offers the ability to noninvasively activate the response in implanted objects while minimizing the heating of surrounding tissue. Second, the heating is achieved by irradiation of a sample by a narrow range of wavelengths. As a result, systems with multiple responses, each activated by a different irradiation wavelength, can be envisioned. Third, the mechanism of activation is independent of polymer chemistry and as a result can be applied to any polymer that exhibits shape memory behavior by phase transitions.

Previous studies have demonstrated the ability to remotely activate shape memory response through indirect heating via SPR excitation in poly(ε-caprolactone) [30, 31], polyurethane (PU) [32, 33], and crosslinked poly(ethylene oxide) [34] SMP. In the present work, an SMP activated by NIR irradiation was developed by the addition of synthesized gold nanorods (AUNR) to a commercial PU, IROGRAN

PS455-203. A simple process for the incorporation of AUNR prepared by the seed-mediated process into the PU SMP is reported. Controlling the shape memory response by altering the irradiation time and intensity and the gold nanorod loading is explored. The effects of AUNR addition on the thermal and shape memory properties are reported.

2. Materials and Methods

2.1. Materials. Gold (III) chloride trihydrate (HAuCl$_4$·3H$_2$0), silver nitrate (AgNO$_3$), L-ascorbic acid, cetyltrimethylammonium bromide (CTAB), and sodium polyacrylate (Na-PAA) were purchased from Sigma-Aldrich. Sodium borohydride (NaBH$_4$) was purchased from Fluka. IROGRAN PS455-203 SMPU pellets were purchased from Huntsman. They contained 9.9% "hard segments" in the form of 4,4'-methylenediphenylene isocyanate and 90.1% of "soft segments" composed of 58.2% butyl diol and 31.8% adipates [35].

2.2. Characterization. UV-vis spectra were collected on a Shimadzu UV-2450 UV-vis spectrophotometer. Absorption spectra were taken from 1000 to 200 nm at a medium speed. For gold solutions, DI-water was used as the reference, and polystyrene cuvettes were used for all samples. Transmission electron microscopy (TEM) was done using a Zeiss EM 10C. Samples were centrifuged for 10 min at 15,500 ×g, and the supernatant was decanted and replaced with DI-water. After repeating the process twice, drops were placed on formvar-coated copper grids and allowed to air dry.

Thermal analysis was performed using the TA Instruments DSC Q2000. A typical procedure utilized a modulated temperature gradient and multiple heating and cooling cycles to capture both the soft and hard phase thermal behavior after annealing. An initial heating and cooling cycle served to anneal the sample; the sample was equilibrated at -80°C and then heated to 100°C at a rate of 10°C/min. The sample was then cooled back to -80°C at a rate of 10°C/min. A second cycle was then performed; the sample was again heated to 100°C at 10°C/min, followed by cooling to -80°C at 10°C/min. Data from the second heating and cooling cycle was used to obtain information regarding the melting and crystallization of the soft segments. Finally, the sample was heated to 200°C at 10°C/min, followed by cooling back down to -80°C at 10°C/min. Data from this cycle was used to obtain information regarding the melting and crystallization of the hard segment.

Mechanical moduli and shape memory behavior (fixity and recovery) were obtained using a TA Instruments DMA RSA III. Moduli were obtained in tensile mode using an initial gauge length of 5 mm and a strain rate of 0.0$\overline{66}$ mm/s to a maximum strain of 300%. Moduli were obtained at multiple temperatures. A multistep process was used to obtain information on fixity and recovery. The temporary shape was set by heating the sample to 60°C, waiting for two minutes, and straining the sample to 300% using a linear deformation rate of 0.0$\overline{66}$ mm/s. The temporary state was set by rapidly quenching the samples to -25°C and holding this temperature for an additional 2 min. The 300% strain was maintained during the quench-and-hold cycle. To obtain fixity, the
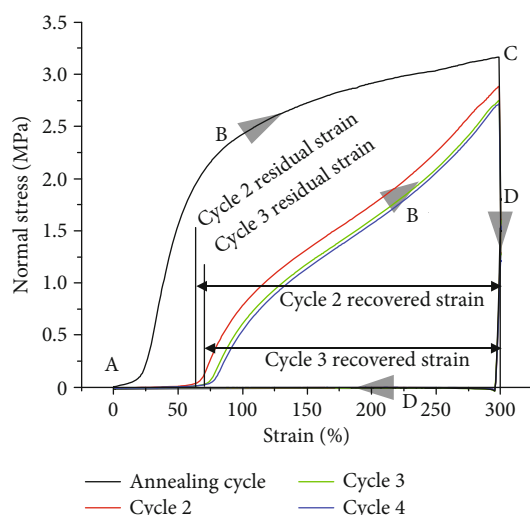
FIGURE 1: Representative DMA testing of shape memory behavior of pure PU films showing multiple cycles of heating (a), strain application (b), quenching (c), and strain recovery (d).

sample was then unloaded. The strain at which the stress returns to zero divided by 300% strain corresponds to the amount of strain "set" in the material, i.e., the fixity. To obtain recovery values, the sample was then heated to 60°C (or other selected temperatures) and held for two minutes. The sample was then strained, and the strain at which the stress increased was recorded. This strain value is called the residual strain and represents strain not recovered by the activation of the shape memory. The ratio of the recovered strain (target set strain (300%) – residual strain) for two cycles is considered the recovery. The initial cycle of set and recovery served to anneal the samples. Data obtained over multiple set and recovery cycles provided insights into changes in behavior due to stress history. Figure 1 is an example of collected data for the unmodified PU films.

2.3. Preparation of Gold Nanorods. Gold nanorods were produced using a seed-mediated surfactant-templating method [36–40] that was optimized to produce rods with longitudinal SPR of ~800-850 nm [29]. In brief, the procedure involved the preparation of spherical seeds that were then "grown" into rods. The seeds were prepared by adding 110 μl of an 8.6 mM $HAuCl_4$ solution to 10 ml of a 0.1 M CTAB in DI-water solution. To this solution, 601 μl of an ice-cold 0.01 M $NaBH_4$ in DI-water was added rapidly. The solution was held at 28°C for two hours. At the end of two hours, a second solution was prepared by adding 130 μl of a 0.01 M $AgNO_3$ solution, 580 μl of a 8.6 mM $HAuCl_4$ solution, and 55 μl of a 0.1 M L-ascorbic acid solution (in that order) to 10 ml of a 0.1 M CTAB in DI-water solution. To this second solution, 96 μl of the previously prepared solution was added. The solution was then kept at 28°C. The solution gradually changed from transparent to light pink over two hours indicating the growth of nanorods. Representative TEM of the prepared rods and their UV-vis spectra are provided in Figure 2. The final solutions contained ~2.0 μg of gold per 10 ml of solution, but conversion to rods was not 100%.

SMP films were prepared by solvent casting from DMF. However, the direct addition of the as-prepared gold rods to a PU DMF solution resulted in dissolution of the PU and poor quality films. Water present in the casting medium acts as an antisolvent in the system, causing phase separation and poor dispersion in the resulting films. Transferring the gold nanoparticles to a DMF solvent and then adding the PU resulted in films with well-dispersed nanoparticles. Xiao et al. reported a similar method [32]. However, the sonication step used by Xiao et al. was not used in the present work as sonication has the potential to break the rods. The as-prepared rods were centrifuged (14,500 ×g for ten minutes), and the supernatant was decanted and replaced with water. This process was repeated twice. After the third centrifugation and decanting, 200 μl of a 17.5 wt% Na-PAA solution was added followed by mixing for 3 min. 15 ml of DMF was then added to the solution. The Na-PAA acts to stabilize the gold nanorods by coating the CTAB bilayer surrounding the rods with a polyelectrolyte [41]. Residual water was removed by evaporation under vacuum at 80°C. The final volume of solution was determined and then made up to 15 ml by the addition of DMF. To this solution, 3.15 g of PU was added, and the solution was mixed and cast into Teflon molds (130 mm × 60 mm × 0.25 mm). The solvent was allowed to evaporate at 80°C overnight.

The total amount of gold used in a single synthesis of rods was 2 μg. When a batch this size was washed, transferred to DMF, and used to cast film from 3.15 g of PU, the final concentration of gold in the film would be ~0.634 ppm. Films using the equivalent of 25% to 500% of a single gold rod batch synthesis were prepared. All gold rod synthesis for the work described here was performed in the same time frame. Each prepared batch was evaluated by UV-vis to confirm the presence of rods and the peak longitudinal absorption. All batches meeting specifications (peak longitudinal absorption between 810 and 840 nm) were then combined to produce a single average "masterbatch" from which samples were taken to produce PU/gold films as described above. Using a masterbatch eliminated the effect of gold nanorod batch variability on the produced film's behavior. While the amount of gold in the films ranged from ~0.2 ppm to ~3.2 ppm, the fraction of gold nanorods was much lower as not all of the gold was conserved during the multiple wash and centrifugation steps, and not all particles were rod shaped.

3. Results and Discussion

In total, five loadings of gold in IROGRAN PS455-203 were prepared: 0, 0.2 ppm, 1.0 ppm, 1.3 ppm, and 3.2 ppm of gold. These values represent the maximum loading of gold in the system. In addition to potential losses during the washing and phase transfer steps, not all of the gold was converted to rods. Orendorff and Murphy estimated that ~15% of the gold is converted to metallic gold [42]. Also, not all the metallic gold was rod shaped, and analysis of several TEM images suggest that roughly 70% of the metallic gold is present as rods and the rest remainder exists as spheres and other
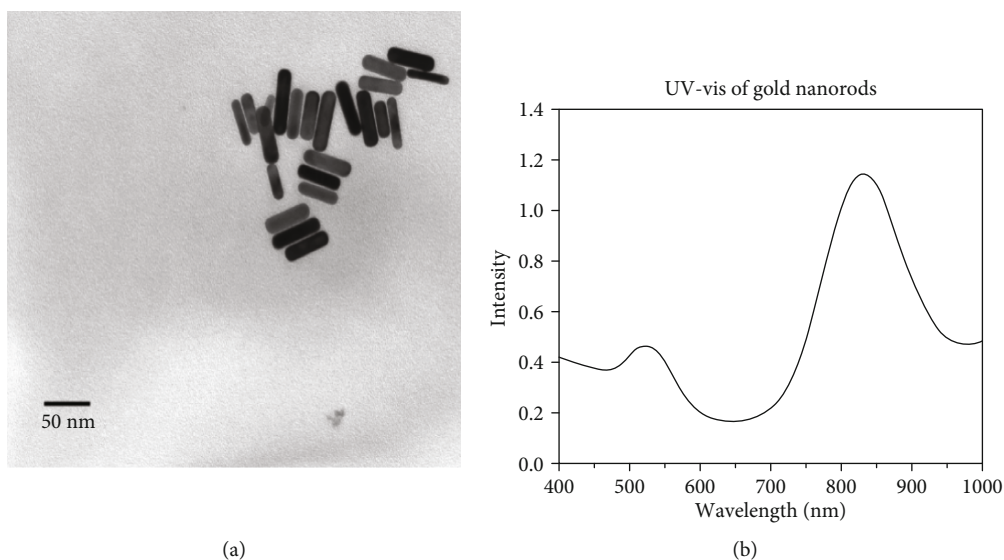
(a)

(b)

FIGURE 2: Prepared gold nanorods: TEM (a) of purified rods with an aspect ratio of ~3.25 and a diameter of ~11.5 nm; UV-vis absorption spectra (b) of purified rods showing a longitudinal absorption peak centered at ~830 nm.
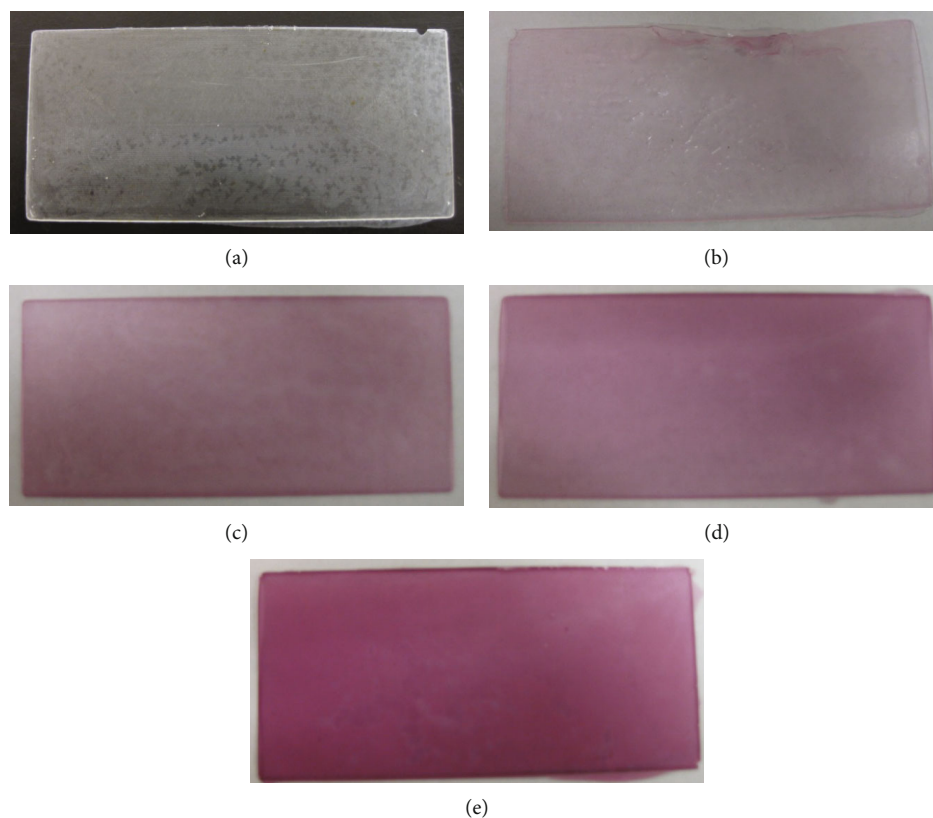

(a)

(b)

(c)

(d)

(e)

FIGURE 3: Representative photos of polyurethane-gold nanorod cast films.

geometries. As a result, the nanorod loading of these samples is roughly 10% of the theoretical gold loading. The photos of these films are shown in Figure 3. The color intensity increases as the gold loading increases.

A key concern was if the addition of AUNR by the method described results in significant changes to properties of the PU composites. Thermal properties of the composites were evaluated to determine if the phase transition temperatures related to the shape memory behavior of these materials were affected. In general, the composites exhibited similar phase transitions to the base PU. Table 1 summarizes the results. The critical phase transition for the shape memory behavior of IROGRAN PS455-203 is the soft segment melting temperature.

TABLE 1: Effects of AUNR loading on thermal transitions and modulus.

AUNR loading (ppm)	T_g (°C)	T_{mSS} (°C)	T_{mHS} (°C)	T_c (°C)	E (MPa)	Fixity (%)	Recovery (%)
0	-32	31	142	51	1.7	98.0	97.5
~0.02	-36	31	143	51	1.5	97.7	93.8
~0.10	-37	31	142	50	1.7	98.5	97.2
~0.13	-35	28	139	51	1.8	98.2	96.9
~0.32	-35	30	137	51	1.7	98.1	96.7

TABLE 2: Recovery as a function of recovery temperature. Recovery ratio is actual recovery divided by the recovery observed at 60°C for the pure PU sample.

Recovery temperature (°C)	Recovery ratio	
	Pure film	0.32 ppm
60	1.00	1.00
50	0.89	0.92
45	0.86	0.88
40	0.83	0.84

TABLE 3: Fixity as a function of quenching temperature. Fixity ratio is actual fixity divided by the fixity observed using a -25°C quenching temperature for the pure PU sample.

Quenching temperature (°C)	Fixity ratio	
	Pure film	0.32 ppm
-25	1.00	0.99
-12	1.01	1.00
0	1.01	0.98
12	0.89	0.92

TABLE 4: Fixity as a function of quenching time. Fixity ratio is actual fixity of a sample divided by the fixity observed using a 600-second quenching time for the pure PU sample.

Quenching time in seconds (s)	Fixity ratio	
	Pure film	0.32 ppm
600	1.00	1.00
300	1.00	1.00
120	0.98	0.98
30	0.93	0.92

This temperature appears to be largely unaffected, as expected, by the addition of the nanoparticles. The T_m of the soft segments (T_{mSS}) of the pure polymer was ~31°C, while for the AUNR-loaded samples, it ranged from ~28 to 31°C with no clear trend. Overall, the melting temperature of the hard segments, a property related to thermal processing, seems to be slightly depressed by the addition of AUNR; T_m for the hard segments (T_{mHS}) in the pure polymer was ~142°C, while for the AUNR-loaded sample it ranged from a high of 143°C (0.02 ppm) to a low of 137°C (0.32 ppm). This behavior can be associated with an interaction of AUNR with the hard segment structures interfering with the crystallization of the hard segments and reducing the melting transition temperature. The soft segments also exhibit a T_g, which was depressed by 3–5°C with the addition of the AUNR. The decrease in T_g could be the result of free volume increase, plasticization, or disruption in the degree of crosslinking created by crystallization of the hard segments [43]. Preferential partitioning of the AUNR particles into the hard phase could result in the decreased T_g and the reduction of T_{mHS} by interfering with the crystallization of the hard phase.

In addition to exploring the effects of AUNR addition on thermal properties of the SMP, the effect of the addition of AUNR on the shape memory performance when the materials are activated in the traditional thermal manner was explored. Recovery and fixity values for films tested using direct heating in the DMA oven are shown in Table 1. In general, the shape memory response was the same for loaded and pure films. The recovery obtained for the 0.02 ppm film was significantly lower than the other samples tested.

Recovery depends on the temperature of the film during the strain recovery process. While any temperature above the T_{mSS} serves to activate the recovery process, higher temperatures lead to faster and more complete relaxation of the amorphous phase, the mechanism for recovery in this system. Table 2 provides the ratio of the observed recovery to the recovery at 60°C for a range of temperatures and both pure PU and 0.32 ppm nanorod-loaded films. In both cases, the recovery decreases with decreasing recovery temperature as expected, and the AUNR-loaded film exhibits very similar behavior to the pure film.

The effect of quenching temperature on fixity was evaluated for the pure and AUNR-loaded films. Table 3 shows the data obtained for pure films and the films loaded with 0.32 ppm of AUNR. As the quenching temperature is increased from -25 to 0°C, the fixity values observed in the films are not affected. However, a quenching temperature of 12°C results in a significant decrease in fixity for both the pure and loaded films. While the T_{mSS} reported in Table 1 is significantly above 12°C, the onset of melting observed was ~0°C. As a result, if any temperature above 0°C is used to set the applied strain, then the fixation is not complete. However, this property is not changed by the addition of AUNR to the system. Quenching time also affects fixity (Table 4). While the films are thin, around 0.2 to 0.25 mm, cooling of the film is not instantaneous. Fully recrystallizing the soft segments is necessary to "lock-in" the applied strain. To evaluate the effect of quenching time, the quenching temperature was held constant at -25°C, and quenching time was varied from a minimum of 30 to a maximum of 600 seconds. For samples quenched for 300 and 600 seconds, no
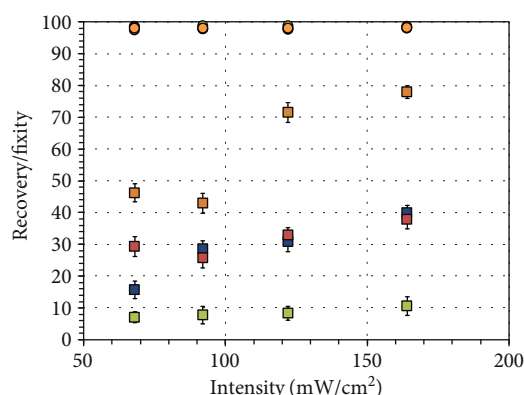
FIGURE 4: Effect of laser output power on recovery (green square: 0.02 ppm; blue square: 0.10 ppm; red square: 0.13 ppm; orange square: 0.32 ppm) and fixity (green circle: 0.02 ppm; blue circle: 0.10 ppm; red circle: 0.13 ppm; orange circle: 0.32 ppm) of polyurethane-AUNR SMPs. Samples identified by estimated loading of gold as nanorods. Error bars are std. error for 5 evaluations.

differences in fixity were observed regardless of the nanorod loading. However, a small reduction in fixity was observed for both pure and composite films at 60 seconds of quenching, and a substantial drop was seen at 30 seconds of quenching time. The effect of quenching time on fixity was similar for the pure and AUNR-loaded films.

The incorporation of low levels of AUNR can be used to impart remote stimulation of shape memory behavior. The effects of irradiation intensity and the rod loading on the photothermal activation of the shape memory behavior for these composites are shown in Figure 4. Irradiation was performed with an LD-WL206 infrared laser from Changchun New Industries Optoelectronics Technology Co. Ltd. The light was directed using a fiber optic cable. The divergence was ~15°; a spot size of roughly 1.5 cm at a distance of 6 cm was observed. Two or three cycles of strain setting and recovery were performed using the oven attached to the DMA as a heat source prior to obtaining data using laser irradiation. The initial cycles allowed for annealing of the sample and collection of baseline fixity and recovery data for comparison. After annealing and baseline data was collected, the samples were irradiated by pointing the fiber optic waveguide at the film from ~6 cm away for 2 min and the sample was then strained to 300% at 0.0$\overline{66}$ mm/s while the sample was continuously irradiated. As quickly as possible, the sample was then quenched to -25°C and held there for 2 min. The strain was returned to zero to obtain fixity. The sample was then irradiated for 2 min from ~6 cm away using the same light source. Then, the sample was strained again to 300% at 0.0$\overline{66}$ mm/s while irradiated to obtain recovery. The ratio of the recovered strain for laser irradiation and the recovered strain for oven heating is considered the efficiency of the photothermal-activated shape memory process. As expected, the efficiency increases as the loading of AUNR increased. Higher rod loading translates into higher efficiency of energy transfer. Higher irradiation intensities also increased efficiency.

4. Conclusions

Under traditional direct heating, the AUNR-loaded films have overall behavior analogous to unloaded films: the addition of AUNR did not significantly affect the mechanical, thermal, or shape memory behavior of the materials. The addition of AUNR did not significantly affect the effects of recovery temperature on recovery, the quenching temperature on fixity, or the quenching time on fixity of the shape memory nanocomposite as compared to the unloaded polyurethane. The photothermally activated shape memory behavior of the nanocomposite was dependent on both AUNR loading and irradiation intensity. Higher loading and higher intensity resulted in a more significant recovery. However, fixity was mostly unaffected by AUNR loading or irradiation intensity in the ranges evaluated.

Data Availability

The TGA, DSC, DMA, SEM, TEM, and UV-vis data used to support the findings of this study are available from the corresponding author upon request.

Conflicts of Interest

The authors declare that there are no conflicts of interest regarding the publication of this manuscript.

Acknowledgments

References

[1] I. A. Rousseau, "Challenges of shape memory polymers: a review of the progress toward overcoming SMP's limitations," *Polymer Engineering and Science*, vol. 48, no. 11, pp. 2075–2089, 2008.

[2] P. T. Mather, X. Luo, and I. A. Rousseau, "Shape memory polymer research," *Annual Review of Materials Research*, vol. 39, no. 1, pp. 445–471, 2009.

[3] M. L. Auad, V. S. Contos, S. Nutt, M. I. Aranguren, and N. E. Marcovich, "Characterization of nanocellulose-reinforced shape memory polyurethanes," *Polymer International*, vol. 57, no. 4, pp. 651–659, 2008.

[4] F. Li, X. Zhang, J. Hou et al., "Studies on thermally stimulated shape memory effect of segmented polyurethanes," *Journal of Applied Polymer Science*, vol. 64, no. 8, pp. 1511–1516, 1997.

[5] M. L. Auad, M. A. Mosiewicki, T. Richardson, M. I. Aranguren, and N. E. Marcovich, "Nanocomposites made from cellulose nanocrystals and tailored segmented polyurethanes," *Journal of Applied Polymer Science*, vol. 115, no. 2, pp. 1215–1225, 2010.

[6] I. S. Gunes and S. C. Jana, "Shape memory polymers and their nanocomposites: a review of science and technology of new

multifinctional materials," *Journal of Nanoscience and Nanotechnology*, vol. 8, no. 4, pp. 1616–1637, 2008.

[7] A. Lendlein and S. Kelch, "Shape-memory polymers," *Angewandte Chemie, International Edition*, vol. 41, no. 12, pp. 2034–2057, 2002.

[8] S. H. Ajili, N. G. Ebrahimi, and M. Soleimani, "Polyurethane/-polycaprolactane blend with shape memory effect as a proposed material for cardiovascular implants," *Acta Biomaterialia*, vol. 5, no. 5, pp. 1519–1530, 2009.

[9] S. Oprea, "Effect of composition and hard-segment content on thermo-mechanical properties of cross-linked polyurethane copolymers," *High Performance Polymers*, vol. 21, no. 3, pp. 353–370, 2009.

[10] P. T. Knight, K. M. Lee, H. Qin, and P. T. Mather, "Biodegradable thermoplastic polyurethanes incorporating polyhedral oligosilsesquioxane," *Biomacromolecules*, vol. 9, no. 9, pp. 2458–2467, 2008.

[11] W. J. Benett, P. A. Krulevitch, A. P. Lee, M. A. Northrup, and J. A. Folta, "Miniature plastic gripper and fabrication method," US Patent 5,609,608, 1997.

[12] D. A. Ferrera, "Shape memory polymer intravascular delivery system with heat transfer medium," US Patent 6,224,610, 2001.

[13] A. P. Lee and J. P. Fitch, "Micro devices using shape memory polymer patches for mated connections," US Patent 6,086,599, 2000.

[14] A. P. Lee, M. A. Northrup, P. E. Ahre, and P. C. Dupuy, "Polymer micromold and fabrication process," US Patent 5,658,515, 1997.

[15] A. P. Lee, M. A. Northrup, D. R. Ciarlo, P. A. Krulevitch, and W. J. Benett, "Release mechanism utilizing shape memory polymer material," US Patent 6,102,933, 2000.

[16] A. Lendlein and R. Langer, "Biodegradable, elastic shape-memory polymers for potential biomedical applications," *Science*, vol. 296, no. 5573, pp. 1673–1676, 2002.

[17] A. Lendlein, M. Behl, B. Hiebl, and C. Wischke, "Shape-memory polymers as a technology platform for biomedical applications," *Expert Review of Medical Devices*, vol. 7, no. 3, pp. 357–379, 2010.

[18] T. J. Lu and A. G. Evans, "Design of a high authority flexural actuator using an electro-strictive polymer," *Sensors and Actuators A: Physical*, vol. 99, no. 3, pp. 290–296, 2002.

[19] P. R. Buckley, G. H. McKinley, T. S. Wilson et al., "Inductively heated shape memory polymer for the magnetic actuation of medical devices," *IEEE Transactions on Biomedical Engineering*, vol. 53, no. 10, pp. 2075–2083, 2006.

[20] C. S. Hazelton, S. C. Arzberger, M. S. Lake, and N. A. Munshi, "RF actuation of a thermoset shape memory polymer with embedded magnetoelectroelastic particles," *Journal of Advanced Materials*, vol. 39, no. 3, pp. 35–39, 2007.

[21] H. Koerner, G. Price, N. A. Pearce, M. Alexander, and R. A. Vaia, "Remotely actuated polymer nanocomposites—stress-recovery of carbon-nanotube-filled thermoplastic elastomers," *Nature Materials*, vol. 3, no. 2, pp. 115–120, 2004.

[22] A. Lendlein, H. Jiang, O. Jünger, and R. Langer, "Light-induced shape-memory polymers," *Nature*, vol. 434, no. 7035, pp. 879–882, 2005.

[23] N. Harris, M. J. Ford, and M. B. Cortie, "Optimization of plasmonic heating by gold nanospheres and nanoshells," *The Journal of Physical Chemistry B*, vol. 110, no. 22, pp. 10701–10707, 2006.

[24] C.-H. Chou, C.-D. Chen, and C. R. C. Wang, "Highly efficient, wavelength-tunable, gold nanoparticle based optothermal nanoconvertors," *The Journal of Physical Chemistry B*, vol. 109, no. 22, pp. 11135–11138, 2005.

[25] W. Hasan, C. L. Stender, M. H. Lee, C. L. Nehl, and J. Lee, "Tailoring the structure of nanopyramids for optimal heat generation," *Nano Letters*, vol. 9, no. 4, pp. 1555–1558, 2009.

[26] A. Mayoral, A. Vazquez-Duran, H. Barron, and M. Jose-Yacaman, "Polyhedral shaped gold nanoparticles with outstanding near-infrared light absorption," *Applied Physics A*, vol. 97, no. 1, pp. 11–18, 2009.

[27] W. Ahn and D. K. Roper, "Transformed gold island film improves light-to-heat transduction of nanoparticles on silica capillaries," *The Journal of Physical Chemistry C*, vol. 112, no. 32, pp. 12214–12218, 2008.

[28] E. S. Kooij, W. Ahmed, C. Hellenthal, H. J. W. Zandvliet, and B. Poelsema, "From nanorods to nanostars: tuning the optical properties of gold nanoparticles," *Colloids and Surfaces A: Physicochemical and Engineering Aspects*, vol. 413, pp. 231–238, 2012.

[29] C. J. Ward, R. Tronndorf, A. S. Eustes, M. L. Auad, and E. W. Davis, "Seed-mediated growth of gold nanorods: limits of length to diameter ratio control," *Journal of Nanomaterials*, vol. 2014, Article ID 765618, 7 pages, 2014.

[30] H. Zhang, H. Xia, and Y. Zhao, "Optically triggered and spatially controllable shape-memory polymer-gold nanoparticle composite materials," *Journal of Materials Chemistry*, vol. 22, no. 3, pp. 845–849, 2012.

[31] Q. Shou, K. Uto, M. Iwanaga, M. Ebara, and T. Aoyagi, "Near-infrared light-responsive shape-memory poly(ε-caprolactone) films that actuate in physiological temperature range," *Polymer Journal*, vol. 46, no. 8, pp. 492–498, 2014.

[32] Z. Xiao, Q. Wu, S. Luo et al., "Shape matters: a gold nanoparticle enabled shape memory polymer triggered by laser irradiation," *Particle & Particle Systems Characterization*, vol. 30, no. 4, pp. 338–345, 2013.

[33] Y. Yao, P. T. Hoang, and T. Liu, "Laser stimulated shape memory polymer with inclusion of gold nanorod—effect of aspect ratio and critical role of on-resonance irradiation," *Journal of Materials Science & Technology*, vol. 33, no. 8, pp. 869–873, 2017.

[34] H. Zhang and Y. Zhao, "Polymers with dual light-triggered functions of shape memory and healing using gold nanoparticles," *ACS Applied Materials & Interfaces*, vol. 5, no. 24, pp. 13069–13075, 2013.

[35] H. Koerner, J. J. Kelley, and R. A. Vaia, "Transient microstructure of low hard segment thermoplastic polyurethane under uniaxial deformation," *Macromolecules*, vol. 41, no. 13, pp. 4709–4716, 2008.

[36] J. Perezjuste, I. Pastorizasantos, L. Lizmarzan, and P. Mulvaney, "Gold nanorods: synthesis, characterization and applications," *Coordination Chemistry Reviews*, vol. 249, no. 17-18, pp. 1870–1901, 2005.

[37] A. V. Alekseeva, V. A. Bogatyrev, B. N. Khlebtsov, A. G. Mel'nikov, L. A. Dykman, and N. G. Khlebtsov, "Gold nanorods: synthesis and optical properties," *Colloid Journal*, vol. 68, no. 6, pp. 661–678, 2006.

[38] N. R. Jana, L. Gearheart, and C. J. Murphy, "Evidence for seed-mediated nucleation in the chemical reduction of gold salts to gold nanoparticles," *Chemistry of Materials*, vol. 13, no. 7, pp. 2313–2322, 2001.

[39] C. J. Murphy, L. B. Thompson, D. J. Chernak et al., "Gold nanorod crystal growth: from seed-mediated synthesis to nanoscale sculpting," *Current Opinion in Colloid & Interface Science*, vol. 16, no. 2, pp. 128–134, 2011.

[40] B. Nikoobakht and M. A. El-Sayed, "Preparation and growth mechanism of gold nanorods (NRs) using seed-mediated growth method," *Chemistry of Materials*, vol. 15, no. 10, pp. 1957–1962, 2003.

[41] A. Gole and C. J. Murphy, "Polyelectrolyte-coated gold nanorods: synthesis, characterization and immobilization," *Chemistry of Materials*, vol. 17, no. 6, pp. 1325–1330, 2005.

[42] C. J. Orendorff and C. J. Murphy, "Quantitation of metal content in the silver-assisted growth of gold nanorods," *The Journal of Physical Chemistry B*, vol. 110, no. 9, pp. 3990–3994, 2006.

[43] D. R. Paul and L. M. Robeson, "Polymer nanotechnology: nanocomposites," *Polymer*, vol. 49, no. 15, pp. 3187–3204, 2008.